Nanoscale

PAPER

View Article Online
View Journal | View Issue



Cite this: *Nanoscale*, 2025, **17**, 5074

# Doping $Gd_{16}$ nanoclusters for expanded optical properties and thermometry applications†

Tingting Li,[a] Jinyu Liu,[a] Feng Jiang,[b] Shengrong He,[b] Jinzhe Liu,[a] Weinan Dong,[b] Ying Zhang,*[c,d] Yanan Li*[c,d] and Zhennan Wu *[b]

Received 14th November 2024,
Accepted 20th January 2025

DOI: 10.1039/d4nr04779f

rsc.li/nanoscale

Lanthanide metal clusters are composed of rigid multinuclear metal cores encapsulated by organic ligands, which have become one of the most interesting research frontiers because of their fantastic architecture, intriguing physical and chemical properties, and potential applications. However, very little attention has been paid to exploring their potential as highly efficient optical materials. $Gd_{16}$ clusters are a new cluster structure that has a rich and varied coordination environment, which is highly conducive to doping and thus controlling luminescence and luminescence color modulation. We achieved green emission by doping $Tb^{3+}$ ions and red emission by doping $Eu^{3+}$ ions in the $Gd_{16}$ cluster structure. Meanwhile, we achieved red–orange–yellow color-tunable luminescence by controlling the composition of $Tb^{3+}$ and $Eu^{3+}$ ions. Studies on the PL properties show that $Gd_{16}$ clusters as the host can be used for doping and efficiently photosensitizing $Tb^{3+}$ ions and $Eu^{3+}$ ions. The existence of energy transfer from the ligand to $Tb^{3+}$ ions and $Eu^{3+}$ ions in the co-doped $Ln_{16}$ clusters was sufficiently demonstrated by time-resolved photoluminescence spectroscopy tests, and the energy transfer efficiency in the clusters was calculated. Furthermore, the temperature-dependent photoluminescence properties of these clusters were investigated to determine their potential as luminescent thermometers.



## Introduction

Lanthanide metal clusters are composed of rigid multinuclear metal cores encapsulated by organic ligands. They perfectly inherit the excellent characteristics of a single lanthanide ion, such as a long luminous life, high luminous color purity, and a large Stokes shift.[1–3] Additionally, they can produce many interesting physical and chemical properties due to the advantages of their structure. For example, they can be used as chemical detection sensors for the fluorescence quenching of some specific functional groups and can be used as optical barcode and temperature sensors by precisely controlling the composition and energy transfer within the clusters.[4,5] Therefore, lanthanide clusters are promising in the field of materials research. However, lanthanide clusters have some disadvantages, such as low luminescence efficiency due to the vibrations of their internal molecules, and their applications need to be further expanded and developed.[6–8]

The emerging $Gd_{16}$ clusters can significantly compensate for these shortcomings.[9] Trifluoroacetylacetone (Tfac) with a suitable triplet-state energy level (22 700 $cm^{-1}$) can effectively sensitize the luminescence of terbium ($Tb^{3+}$) and europium ($Eu^{3+}$) ions.[10,11] Secondly, the C–F bond in trifluoroacetylacetone can effectively inhibit the molecular vibrations in the clusters and improve the luminous efficiency.[12] More importantly, $Gd_{16}$ has multiple sites and a rich coordination environment, which provides abundant sites for doping. Thus, $Gd_{16}$ clusters are an excellent substrate material. On this basis, red light emission is realized by doping $Gd_{16}$ clusters with $Eu^{3+}$ ions. Green emission is realized by doping $Gd_{16}$ clusters with $Tb^{3+}$ ions. By co-doping $Gd_{16}$ clusters with $Tb^{3+}$ and $Eu^{3+}$ ions and precisely regulating the content of terbium and europium ions, the emission of clusters from red light to yellow light can be tuned. The energy transfer from $Tb^{3+}$ ions to $Eu^{3+}$ ions was confirmed by measuring the decay lifetime of $Tb^{3+}$ ions in the co-doped structure.[13,14]

Due to the tunable luminescence in the co-doped structure, we further investigated its temperature-dependent photoluminescence properties.[15–17] These were evaluated using variable-temperature spectroscopy, revealing that the emitted

[a]*School of Materials Science and Engineering, Jilin Jianzhu University, Changchun 130018, China*
[b]*State Key Laboratory of Integrated Optoelectronics and College of Electronic Science and Engineering, Jilin University, Changchun 130012, China. E-mail: Wuzn@jlu.edu.cn*
[c]*Department of Paediatrics, Children's Medical Center, The First Hospital of Jilin University, Changchun 130021, China. E-mail: ynli@jlu.edu.cn, yingzhang@jlu.edu.cn*
[d]*Clinical Research Center for Child Health, The First Hospital of Jilin University, Changchun 130021, China*

† Electronic supplementary information (ESI) available. See DOI: https://doi.org/10.1039/d4nr04779f

colors exhibit notable temperature sensitivity. By fitting the variable-temperature spectra, the relative sensitivity ($S_r$) was determined to be 4.6% $K^{-1}$, which is among the highest reported in the literature. This indicates promising potential for its application in luminescent thermometers.

## Results and discussion

The lanthanide metal clusters $Gd_{16}$ were synthesized according to previous work.[9] Analysis of single-crystal structures showed that the compound $Gd_{16}$ crystallizes in the $C_2/m$ space group within a monoclinic crystal system. The $Gd_{16}$ cluster comprises 16 $Gd^{3+}$ ions coordinated to 20 trifluoroacetylacetone (TFac) ligands, 8 methanol molecules, 24 $\mu_3$-OH bridging groups, and 2 $\mu_6$-O bridging groups. The $Gd^{3+}$ ions are interconnected through $\mu_3$-OH and $\mu_6$-O bridging groups, facilitating the formation of two distinct structural units. In particular, six $Gd^{3+}$ ions are linked to eight $\mu_3$-OH groups, resulting in the formation of the structural unit $[Gd_6(\mu_3\text{-}OH)_8]^{10+}$ (Fig. 1a). The incorporation of $\mu_6$-O bridging ligands further generates the second structural unit, $[Gd_6(\mu_3\text{-}OH)_8(\mu_6\text{-}O)]^{8+}$(Fig. 1b). Two units are further integrated into the $Gd_{16}$ cluster through the sharing of a central $Gd^{3+}$ ion. The coordination sphere of the cluster is completed by the coordination of 20 TFac ligands and 8 methanol molecules (Fig. 1c). The Gd1 and Gd6 ions exhibit a nine-coordinate capped square antiprism geometry, whereas Gd2/Gd3/Gd4/Gd5 ions adopt an eight-coordinate biaugmented trigonal prism geometry (Fig. 1d). The coordinating oxygen atoms are derived from TFac ligands, $\mu_3$-OH bridging groups, and $\mu_6$-O bridging groups. The Gd–O bond lengths range from 2.420(1) to 2.450(3) Å, aligning well with previously published studies. Notably, the TFac ligands coordinate with individual $Gd^{3+}$ ions in a chelating bidentate mode and, together with the methanol molecules, exhibit three distinct coordination environments (Fig S1†). Crystal data are summarized in Table S16.† In Fig S2,† the powder X-ray diffraction (PXRD) patterns for the $\mathbf{Gd_{16-x}Eu_x}$, $\mathbf{Gd_{16-x}Tb_x}$ and $\mathbf{Gd_{15}Tb_{1-x}Eu_x}$ ($x$ = 0.2, 0.4, 0.6, 0.8) samples are shown. The atomic content in these samples were proved *via* ICP-OES (Table S1†). The observed diffraction peaks predominantly correspond to the $Gd_{16}$ phase, indicating that the incorporation of dopant ions did not induce significant alterations in the crystalline structure. Furthermore, the subtle variations in peak positions among the different clusters are indicative of minor changes in the crystal lattice parameters, attributed to the differing concentrations of the doped lanthanide ions.

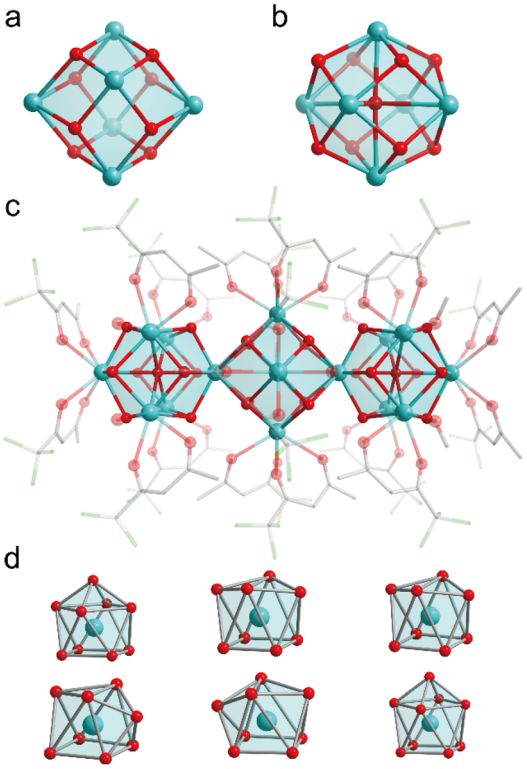


**Fig. 1** (a) Ball-and-stick representation of $[Gd_6(\mu_3\text{-}OH)_8]^{10+}$. (b) Ball-and-stick representation of $[Gd_6(\mu_3\text{-}OH)_8(\mu_6\text{-}O)]^{8+}$ (c) Ball-and-stick representation of $[Gd_{16}(tfac)_{20}(CH_3OH)_8(\mu_3\text{-}OH)_{24}(\mu_6\text{-}O)_2]$. (d) The coordination geometries of $Gd^{3+}$.

The luminescence of lanthanide ions is typically excited *via* the antenna effect of the coordinating ligands. However, for $Gd^{3+}$, efficient excitation *via* the ligand's antenna effect is challenging due to its high resonance energy levels. To enhance the luminescence of $Gd^{3+}$-based clusters, doping with optically active ions provides a viable strategy. In the case of $Gd_{15.2}Eu_{0.8}$, the excitation spectrum reveals a significant absorption band around 335 nm (Fig. 2a), which can be attributed to the ligand $^1\pi \rightarrow {}^1\pi^*/{}^3\pi^*$ charge transfer transition. Here, $^1\pi$, $^1\pi^*$, and $^3\pi^*$ represent the ground state, the first excited singlet state, and the first excited triplet state, respectively.[18] Upon excitation at 336 nm, the emission spectrum exhibits four distinct peaks at 595 nm, 615 nm, 655 nm, and 695 nm, corresponding to the $^5D_0 \rightarrow {}^7F_1$, $^5D_0 \rightarrow {}^7F_2$, $^5D_0 \rightarrow {}^7F_3$ and $^5D_0 \rightarrow {}^7F_4$ transitions of $Eu^{3+}$ (Fig. 2b). This indicates that the $tfac^-$ ligand effectively

**Zhennan Wu**

*Zhennan Wu joined Jilin University in 2021 and is currently a full professor at the College of Electronic Science and Engineering. He obtained his Ph. D. degree (2016) from the State Key Laboratory of Supramolecular Structure and Materials at Jilin University under the supervision of Prof. Hao Zhang. Thereafter, he joined the team of Prof. Osman. M. Bakr in KAUST (2016–2018) and Prof. Xie Jianping in NUS (2018–2020) for post-doctoral research. His research interests are colloidal synthesis dynamics, self-assembly chemistry, optical physics, and photoelectric devices of metal nanoclusters.*

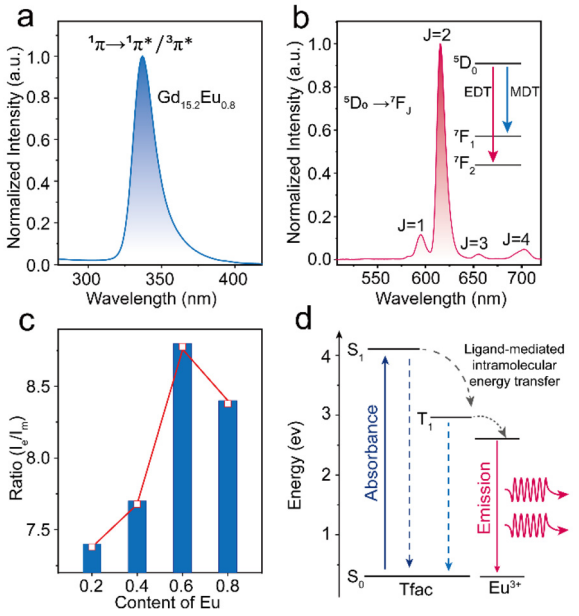


**Fig. 2** (a) The excitation spectra of $Gd_{15.2}Eu_{0.8}$. (b) The emission spectra of $Gd_{15.2}Eu_{0.8}$. (c) Trend curve of $I_e/I_m$ in different $Eu^{3+}$ ratios. (d) Diagram of the energy transfer mechanism.

facilitates the sensitization of $Eu^{3+}$ in these clusters.[19–21] The clusters exhibit a characteristic red emission, as depicted in the CIE chromaticity diagram (Fig. S4†). Additionally, the dependence of photoluminescence on doping concentration was explored (Fig. S5†). The intensity of the $Eu^{3+}$ intrinsic transitions increases significantly with the doping concentration, suggesting that higher doping levels promote more efficient energy transfer from the ligand to $Eu^{3+}$ ions.

The coordination environment significantly influences the physical properties of compounds, and $Gd_{16}$, with its atomically defined structure, offers a well-controlled system for investigating these effects. Among the four characteristic transitions of $Eu^{3+}$ the $^5D_0 \rightarrow {}^7F_1$ transition is a magnetic dipole transition, which is insensitive to the symmetry of the $Eu^{3+}$ coordination sphere.[22,23] In contrast, the $^5D_0 \rightarrow {}^7F_2$ transition is an electric dipole transition, which is highly dependent on the symmetry of the $Eu^{3+}$ local lattice environment. From the emission spectra, the intensities of the electric dipole transition ($I_e$) at 615 nm and the magnetic dipole transition ($I_m$) at 595 nm were derived for the samples $Gd_{15.8}Eu_{0.2}$, $Gd_{15.6}Eu_{0.4}$, $Gd_{15.4}Eu_{0.6}$, $Gd_{15.2}Eu_{0.8}$ (Fig. 2c). As the doping concentration increases, the ratio of $I_e/I_m$ progressively increases, which suggests a reduction in the symmetry of the $Eu^{3+}$ coordination sites. This reduction in symmetry is further linked to changes in energy transfer efficiency, and theoretical calculations were performed to quantify these effects (Fig. 2d and Table S2–12†).[24] The analysis of the forward rate ($W^T$) and backward rate ($W_B^T$) constants for the two representative samples, as shown in Table S3,† reveals that the difference between $W^T$ and $W_B^T$ for $Gd_{15.4}Eu_{0.6}$ is smaller than for $Gd_{15.2}Eu_{0.8}$, suggesting that the latter exhibits more efficient luminescence. These results indicate that the emission intensity of the clusters is influenced by both the symmetry of the lattice and the dynamics of energy transfer, with the latter exerting a more dominant influence. In a similar manner, the $Tb^{3+}$ doped $Gd_{16}$ clusters also exhibit notable sensitization characteristics, which further highlight the versatility of the coordination environment in modulating the photoluminescence properties. The emission spectra, obtained under 336 nm excitation, show four characteristic peaks at 492 nm, 547 nm, 587 nm, and 623 nm, which correspond to the $^5D_4 \rightarrow {}^7F_6$, $^5D_4 \rightarrow {}^7F_5$, $^5D_4 \rightarrow {}^7F_4$, and $^5D_4 \rightarrow {}^7F_3$ transitions of $Tb^{3+}$ (Fig. S6 & S7†).[25] The corresponding CIE chromaticity diagrams indicate that the emission is predominantly in the green region (Fig. S8†). As with $Eu^{3+}$ doped $Gd_{16}$, the photoluminescence properties of $Tb^{3+}$ doped samples exhibit a dependence on doping concentration and the coordination environment, showing trends similar to those observed for $Eu^{3+}$ doping (Fig. S9†). These results further support the notion that the ligands in $Gd_{16}$ possess strong sensitization ability, which can be leveraged to expand the optical properties of the material.

The efficient energy transfer between the ligand and $Tb^{3+}$/$Eu^{3+}$ ions, coupled with their distinct emission colours, offers significant potential for achieving a wide range of colour-tuning through co-doping and modulation of ion concentrations.[26] Doping $Gd_{16}$ clusters with $Eu^{3+}$ and $Tb^{3+}$ respectively can make $Gd_{15}Eu_{1-x}$ and $Gd_{15}Tb_{1-x}$ show red or green fluorescence colour (Fig. 3b). The emission spectra of $\mathbf{Gd_{15}Tb_{1-x}Eu_x}$ ($x$ = 0.2, 0.4, 0.6, 0.8) confirmed the effective sensitization of the ligand and display both the characteristic emissions of $Tb^{3+}$ ions and $Eu^{3+}$ ions (Fig. 3b). Notably, the emission profile of $\mathbf{Gd_{15}Tb_{1-x}Eu_x}$ can be finely tuned through the variation of $Eu^{3+}$ doping, resulting in a shift from yellow to red emission. It is noteworthy that increasing the concentration of $Eu^{3+}$ ions enhances the relative intensity of $Eu^{3+}$ emission relative to that of $Tb^{3+}$, thereby allowing for precise control over the color-tuning of the emission output. In the co-doped $Gd_{16}$ clusters with $Tb^{3+}$ and $Eu^{3+}$, revealed that the spacing between the $Ln^{3+}$ ions is less than 10 Å, which facilitates effective energy transfer.[27] To demonstrate the energy transfer of $Tb^{3+} \rightarrow Eu^{3+}$, we investigated the emission decay $^5D_4 \rightarrow {}^7F_5$ transition of $Tb^{3+}$ at 547 nm (Fig. 3c and S10†). A comparison of the emission lifetimes of the donor ion ($Tb^{3+}$) in the presence and absence of the acceptor ion ($Eu^{3+}$) (Table S13†) revealed that the luminescence lifetime of $Tb^{3+}$ decreases in the presence of $Eu^{3+}$, providing strong evidence for the $Tb^{3+} \rightarrow Eu^{3+}$ energy transfer process. To further illustrate the energy transfer mechanism from $Tb^{3+}$ to $Eu^{3+}$ ions, we have provided a schematic diagram of the process in $\mathbf{Gd_{15}Tb_{1-x}Eu_x}$ ($x$ = 0.2, 0.4, 0.6, 0.8) clusters, based on the work of Crosby and Whan (Fig. S11†).[28] Upon excitation of the $tfac^-$ ligand from the ground state, it undergoes intersystem crossing to the $T_1$ (first excited triplet state) energy level. The energy in $T_1$ then relaxes to the $^5D_4$ energy level of the $Tb^{3+}$ ion which subsequently relaxes to the

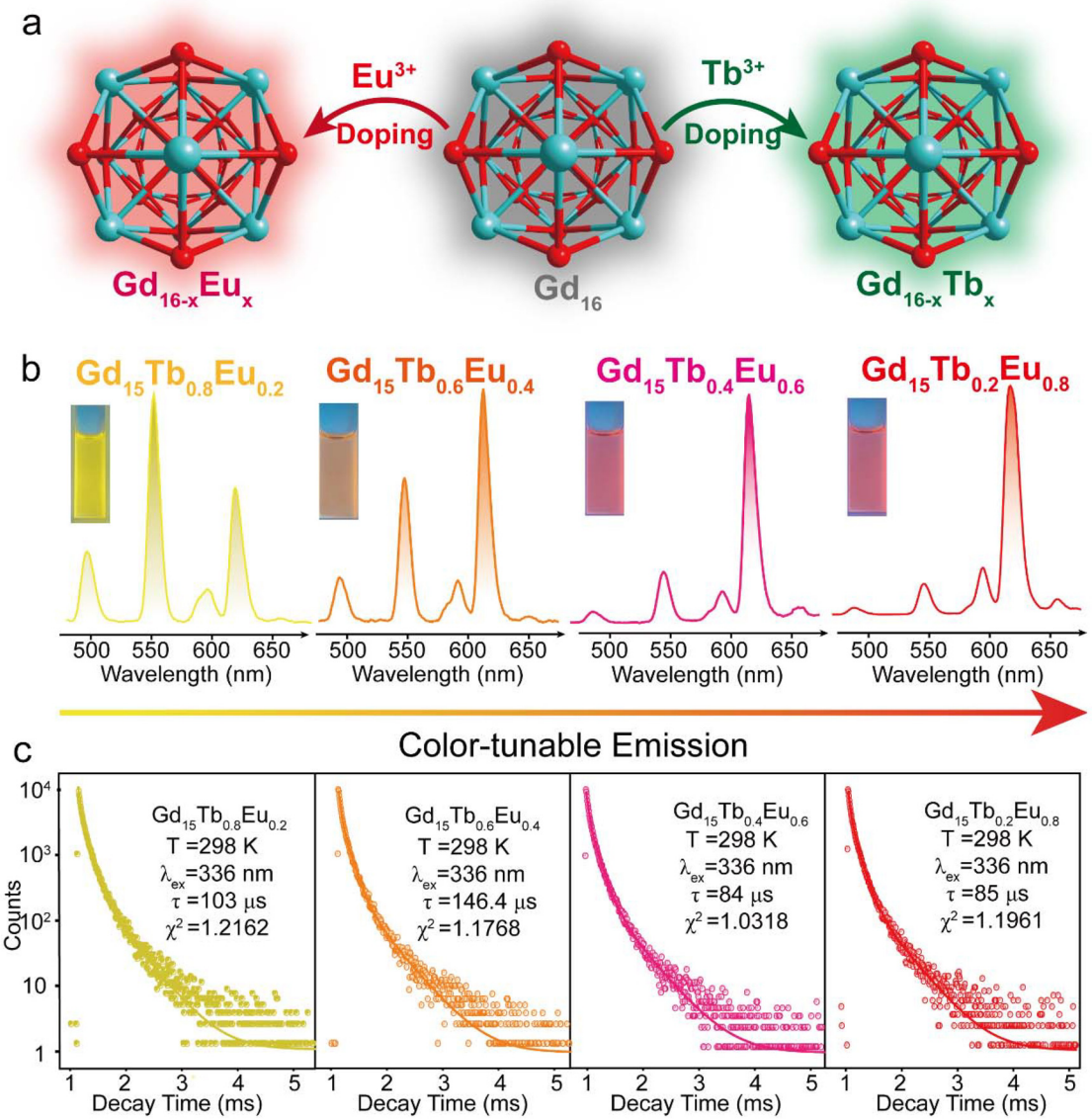


**Fig. 3** (a) Schematic illustration of fluorescence colour modulation in $Gd_{16}$ clusters upon doping with $Eu^{3+}$ and $Tb^{3+}$ ions. (b) The emission spectra of $\mathbf{Gd_{15}Tb_{1-x}Eu_x}$ ($x$ = 0.2, 0.4, 0.6, 0.8) clusters. (c) The emission decay lifetimes of $^5D_4 \rightarrow {}^7F_5$ transition of $Tb^{3+}$ at 547 nm in $\mathbf{Gd_{15}Tb_{1-x}Eu_x}$ ($x$ = 0.2, 0.4, 0.6, 0.8) clusters.

ground state, emitting characteristic $Tb^{3+}$ luminescence. Simultaneously, energy is transferred from the $^5D_4$ level of $Tb^{3+}$ to the $^5D_1$ level of $Eu^{3+}$, which then relaxes to the ground state, producing the characteristic $Eu^{3+}$ emission. This dual emission from both $Tb^{3+}$ and $Eu^{3+}$ ions results in the observed dual-color output.

$$\langle \eta_{Tb\rightarrow Eu} \rangle \% = \left[1 - \left(\frac{\tau}{\tau_0}\right)\right] \times 100 \quad (1)$$

Meanwhile, to calculate the energy transfer efficiency between $Tb^{3+} \rightarrow Eu^{3+}$ in clusters, we use the formula proposed by Piguet and colleagues to calculate the energy transfer efficiency of $Tb^{3+} \rightarrow Eu^{3+}$(eqn (1)) (Table. S13†), where $\tau$ denotes the luminescence lifetime of $Tb^{3+}$ in the presence of the host ion and $\tau_0$ denotes the luminescence lifetime of $Tb^{3+}$ in the absence of the host ion.[13] Analysis of the excited-state lifetimes of the cluster within the framework of the Förster theory of energy transfer showed that the transfer has an efficiency of ~12%.

$$\Delta = \frac{A_1 - A_2}{1 + e^{(T-T_0)}/dT} + A_2 \quad (2)$$

$$S_r(\%) = \left[\frac{\partial\Delta/\partial T}{\Delta}\right] \times 100 \quad (3)$$

Lanthanide clusters incorporating both $Tb^{3+}$ and $Eu^{3+}$ ions are theoretically highly sensitive to temperature changes

due to their dual-emission features.[29] To investigate the potential of $\mathbf{Gd_{15}Tb_{1-x}Eu_x}$ ($x$ = 0.2, 0.4, 0.6, 0.8) clusters as luminescent temperature sensors, temperature-dependent emission spectra of $Gd_{15}Tb_{0.2}Eu_{0.8}$ were recorded. In the temperature range of 80–160 K, the intensities of the characteristic emission peaks of both $Tb^{3+}$ and $Eu^{3+}$ remained relatively stable, likely due to the suppression of non-radiative relaxation at lower temperatures (Fig. 4a). However, between 160 and 300 K, the intensities of these emission peaks gradually decreased, suggesting that increased temperature enhances non-radiative relaxation (Fig. 4c). The temperature-dependent emission spectra of $Gd_{15}Tb_{0.8}Eu_{0.2}$ were analyzed, showing similar trends (Fig. 4b). In the 80–160 K range, the emission peaks of $Eu^{3+}$ ions and $Tb^{3+}$ ions remained relatively constant. At higher temperatures (160–300 K), the $Tb^{3+}$ emission intensity decreased continuously, while the $Eu^{3+}$ emission intensity initially increased before also decreasing (Fig. 4d). This behavior can be attributed to energy transfer from $Tb^{3+}$ to $Eu^{3+}$, which boosts the $Eu^{3+}$ emission peak. However, as the temperature continues to increase, the energy transfer becomes insufficient to compensate for the non-radiative relaxation losses in $Eu^{3+}$, causing its emission peak to decline. In the $Gd_{15}Tb_{0.2}Eu_{0.8}$ cluster, although energy transfer from $Tb^{3+}$ to $Eu^{3+}$ also occurs, the low concentration of $Tb^{3+}$ ions in this material is not sufficient to offset the energy loss from non-radiative relaxation in $Eu^{3+}$. To assess the sensitivity of $Gd_{15}Tb_{0.2}Eu_{0.8}$ and $Gd_{15}Tb_{0.8}Eu_{0.2}$ as luminescent thermometers, the relative sensitivity, a key parameter for evaluating performance, was calculated.[30] The relative sensitivity was derived by fitting the ratio $\Delta$ using the Boltzmann function (eqn (2), Fig. 4e & f),[31,32] with relevant fitting parameters listed in Table S14† (where $\Delta = I_1/I_2$, $I_1$ represents the peak emission intensity of $Tb^{3+}$ at 547 nm and $I_2$ represents the peak emission intensity of $Eu^{3+}$ at 615 nm). The relative sensitivities corresponding to the $\mathbf{Gd_{15}Tb_{1-x}Eu_x}$ ($x$ = 0.2, 0.8) clusters can be obtained by applying eqn (3) to the fitted Boltzmann function (Fig. 4e & f).[33] The relative sensitivities of these clusters increase with temperature, exhibiting high sensitivities at 300 K (relative sensitivities 3.7% $K^{-1}$ and 4.6% $K^{-1}$, respectively), demonstrating their potential as light-emitting thermometers.

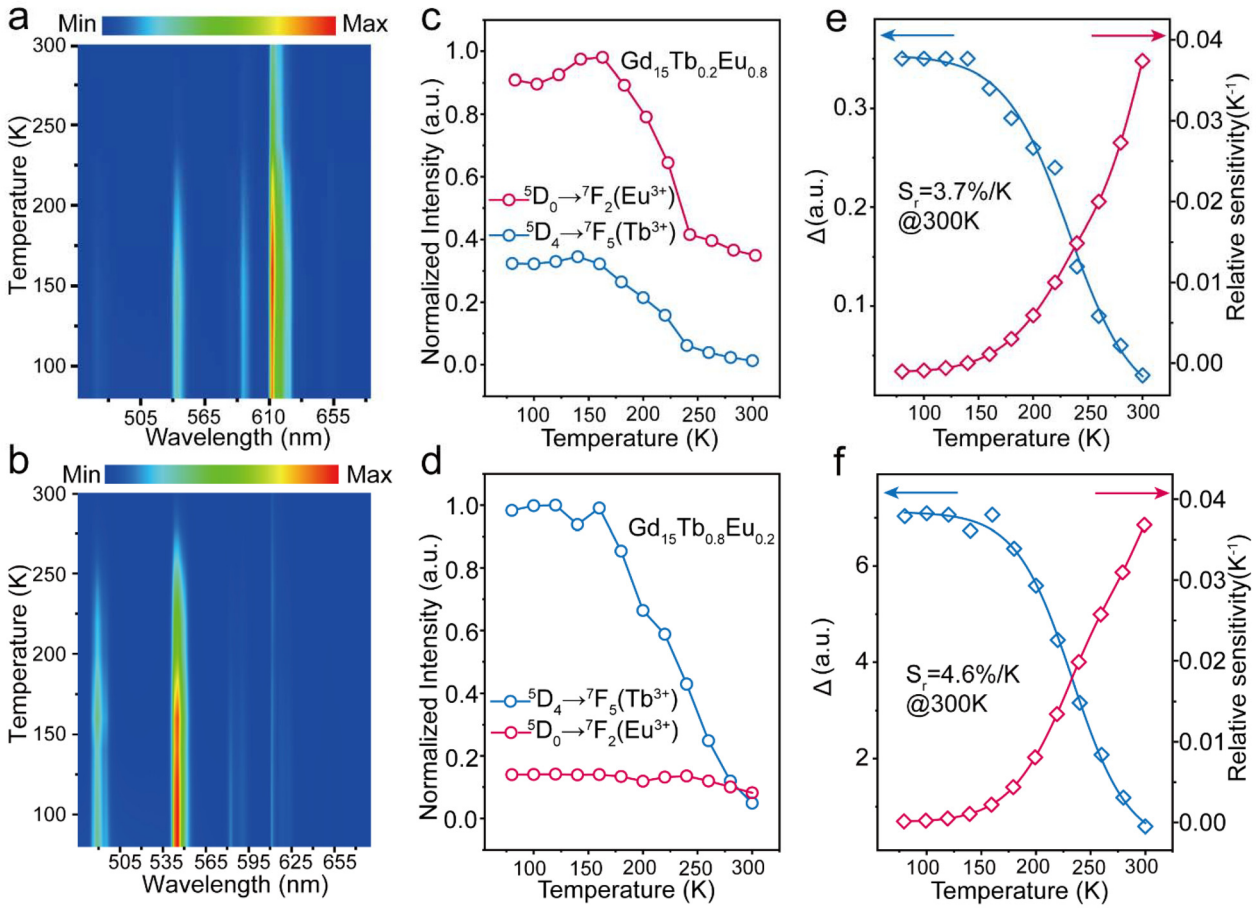


**Fig. 4** (a) Temperature-dependent photoluminescence spectra of $Gd_{15}Tb_{0.2}Eu_{0.8}$. (b) Temperature-dependent photoluminescence spectra of $Gd_{15}Tb_{0.8}Eu_{0.2}$. (c) The intensity changes of emission peaks for $Eu^{3+}/Tb^{3+}$ in $Gd_{15}Tb_{0.2}Eu_{0.8}$. (d) The intensity changes of emission peaks for $Eu^{3+}/Tb^{3+}$ in $Gd_{15}Tb_{0.8}Eu_{0.2}$. (e) The temperature dependence of the thermometric parameter ($\Delta$) of $Gd_{15}Tb_{0.2}Eu_{0.8}$ (lines represent the fitted function). (f) The temperature dependence of the thermometric parameter ($\Delta$) of $Gd_{15}Tb_{0.8}Eu_{0.2}$ (lines represent the fitted function).

## Conclusions

In conclusion, green emission was achieved by doping $Tb^{3+}$ ions and red emission was achieved by doping $Eu^{3+}$ ions into the $Gd_{16}$ cluster. By co-doping with $Tb^{3+}$ and $Eu^{3+}$ ions adjusting their concentrations, we obtained red–orange–yellow color-tunable luminescence in $Gd_{16}$ clusters. Photoluminescence studies demonstrated that $Gd_{16}$ effectively serves as a host for the efficient photosensitization of both $Tb^{3+}$ and $Eu^{3+}$ ions. The energy transfer from the ligand to $Tb^{3+}$ and $Eu^{3+}$ ions in the co-doped $Gd_{16}$ clusters was confirmed through temperature-resolved photoluminescence measurements, and the energy transfer efficiency was calculated. Additionally, the temperature-dependent photoluminescence properties of these clusters were examined to assess their potential as luminescent thermometers. Overall, this work significantly advances the field of rare earth metal clusters by enabling tunable color emissions in $Gd_{16}$ clusters.

## Experimental section

## Materials and methods

All chemicals were used as is without further purification. Powder XRD patterns were obtained using a Rigaku Ultima IV diffractometer with a Cu source. Photoluminescence excitation (PLE) and photoluminescence (PL) were measured on a Hitachi F-4700 spectrometer with excitation and emission slits of 2.5 nm. Other parameters: scan speed 240 nm $min^{-1}$, PMT voltage 700 V, and response 2.0 s. The temperature change test and emission decay life of all samples measurement were conducted on an FLS1000 spectrofluorometer (Edinburgh Instruments Ltd). FTIR spectra were obtained using a Nicolet 6700 FTIR spectrometer in ATR mode (Fig. S3†). ICP-OES analysis was performed with an Agilent 5110 ICP-OES instrument.

### Synthesis of $Gd_{16-x}Eu_x$ ($x$ = 0.2; 0.4; 0.6; 0.8)

The synthesis of this series of lanthanide clusters follows a similar procedure.[9] A mixture of (16-$x$)/16 mmol of Gd $(NO_3)_3{\cdot}6H_2O$ and $x$/16 mmol of $Eu(NO_3)_3{\cdot}6H_2O$ were dissolved in a mixture of $CH_3CN$ (2 mL) and $CH_3OH$ (1 mL) at ambient temperature with continuous stirring to ensure complete solvation. Trifluoroacetylacetone (2 mmol, 245 μL) was subsequently added, and the solution was stirred for 7–8 minutes. Triethylamine (4.4 mmol, 550 μL) was then introduced as a base, and the mixture was stirred for an additional 4–5 minutes. The reaction mixture was then filtered, stored at 4–8 °C, and allowed to evaporate slowly, yielding crystals within one week. Selected IR peaks ($cm^{-1}$): 3433(s), 2993(w), 2935(w), 1639(s), 1527(s), 1473(s), 1363(s), 1290(s), 1228(m), 1189(m), 1137(s), 1016(m), 945(m), 854(s), 779(s), 727(s), 673(m), 613(w), 559(s).

### Synthesis of $Gd_{16-x}Tb_x$ ($x$ = 0.2; 0.4; 0.6; 0.8)

Compounds $Gd_{16-x}Tb_x$ were prepared using the same procedures as described above for the synthesis of compounds $Gd_{16-x}Eu_x$ but replacing $Eu(NO_3)_3{\cdot}6H_2O$ with $Tb(NO_3)_3{\cdot}6H_2O$. After one week of solvent evaporation at 4–8 °C, colorless crystals were obtained. Selected IR peaks ($cm^{-1}$): 3433(s), 2993(w), 2935(w), 1639(s), 1527(s), 1473(s), 1363(s), 1290(s), 1228(m), 1189(m), 1137(s), 1016(m), 945(m), 854(s), 779(s), 727(s), 673(m), 613(w), 559(s).

### Synthesis of $Gd_{15}Tb_{1-x}Eu_x$ ($x$ = 0.2; 0.4; 0.6; 0.8)

Compounds $Gd_{15}Tb_{1-x}Eu_x$ were prepared using the same procedures as described above for the synthesis of compounds $Gd_{16-x}Eu_x$ but replacing $Eu(NO_3)_3{\cdot}6H_2O$ with 0.9375 mmol Gd $(NO_3)_3{\cdot}6H_2O$, (1 − $x$)/16 mmol of $Tb(NO_3)_3{\cdot}6H_2O$ and $x$/16 mmol of $Eu(NO_3)_3{\cdot}6H_2O$. After one week of solvent evaporation at 4–8 °C, colorless crystals were obtained. Selected IR peaks ($cm^{-1}$): 3433(s), 2993(w), 2935(w), 1639(s), 1527(s), 1473(s), 1363(s), 1290(s), 1228(m), 1189(m), 1137(s), 1016(m), 945(m), 854(s), 779(s), 727(s), 673(m), 613(w), 559(s).

## Data availability

The authors confirm that the data supporting the findings of this study are available within the article and its ESI.†

## Conflicts of interest

There are no conflicts to declare.

## Acknowledgements

This work was supported by the National Natural Science Foundation of China (12174151 and 12304448).

## References

1 Y. Wang, Y. Yang, F. Gao, X. Zhang, L. Zhu, H. Yan, P. Yang and M. Gao, *Angew. Chem., Int. Ed.*, 2024, **63**, e202407613.
2 S. V. Eliseeva and J. C. G. Bünzli, *Chem. Soc. Rev.*, 2010, **39**, 189–227.
3 J. Jiang, Y. Xu, W. Yang, R. Guan, Z. Liu, H. Zhen and Y. Cao, *Adv. Mater.*, 2006, **18**, 1769–1773.
4 T. Li, J. Liu, S. Zheng, F. Jiang, J. Liu, W. Dong, Y. Zhang, S. Zheng, Y. Li, Z. Wu and X. Bai, *Rare Met.*, 2024, **42**, DOI: 10.1007/s12598-024-03090-0.
5 W. Lustig and J. Li, *Coord. Chem. Rev.*, 2018, **373**, 116–147.
6 C. Wang, X. Yang, S. Wang, T. Zhu, L. Bo, L. Zhang, H. Chen, D. Jiang, X. Dong and S. Huang, *J. Mater. Chem. C*, 2018, **6**, 865–874.
7 Y. Cui, Y. Yue, G. Qian and B. Chen, *Chem. Rev.*, 2012, **112**, 1126–1162.

8 S. Sculfort and P. Braunstein, *Chem. Soc. Rev.*, 2011, **40**, 2741–2760.
9 M. Du, L. Chen, L. Jiang, W. Liu, L. Long, L. Zheng and X. Kong, *J. Am. Chem. Soc.*, 2022, **144**, 5653–5660.
10 W. Liu, G. Li, H. Xu, M. Du, L. Long, L. Zheng and X. Kong, *Inorg. Chem.*, 2022, **61**, 9849–9854.
11 S. Rentschler, H. Linn, K. Deininger, M. T. Bedford, X. Espanel and M. Sudol, *Biol. Chem.*, 1999, **380**, 431–442.
12 S. Mishra and S. Daniele, *Chem. Rev.*, 2015, **115**, 8379–8448.
13 H. Yao, G. Calvez, C. Daiguebonne, K. Bernot, Y. Suffren and O. Guillou, *Inorg. Chem.*, 2019, **58**, 16180–16193.
14 J. I. Deneff, L. E. S. Rohwer, K. S. Butler, B. Kaehr, D. J. Vogel, T. S. Luk, R. A. Reyes, A. A. Cruz-Cabrera, J. E. Martin and D. F. S. Gallis, *Nat. Commun.*, 2023, **14**, 981.
15 Y. Cui, R. Song, J. Yu, M. Liu, Z. Wang, C. Wu, Y. Yang, B. Chen and G. Qian, *Adv. Mater.*, 2015, **27**, 1420–1425.
16 D. Zhao, D. Yue, K. Jiang, Y. Cui, Q. Zhang, Y. Yang and G. Qian, *J. Mater. Chem. C*, 2017, **5**, 1607–1613.
17 S. He, H. Xu, C. Chen, X. Wang, T. Lu, L. Cao, J. Zheng and X. Zheng, *Nanoscale*, 2023, **15**, 15730–15738.
18 H. Yao, G. Calvez, C. Daiguebonne, Y. Suffren, K. Bernot and O. Guillou, *Inorg. Chem.*, 2021, **60**, 16782–16793.
19 Y. Pointel, F. Houard, Y. Suffren, C. Daiguebonne, F. L. Natur, S. Freslon, G. Calvez, K. Bernot and O. Guillou, *Inorg. Chem.*, 2020, **59**, 11028–11040.
20 H. Yao, G. Calvez, C. Daiguebonne, K. Bernot, Y. Suffren, M. Puget, C. Lescop and O. Guillou, *Inorg. Chem.*, 2017, **56**, 14632–14642.
21 Y. Zhao, H. Zheng, L. Chen, H. Chen, X. Kong, L. Long and L. Zheng, *Inorg. Chem.*, 2019, **58**, 10078–10083.
22 R. Ilmi and K. Iftikhar, *Polyhedron*, 2015, **102**, 16–26.
23 F. Cagnin, M. R. Davolos and E. E. Castellano, *Polyhedron*, 2014, **67**, 65–72.
24 L. Yan, Y. Zhang, T. Zhang, Y. Feng, K. Zhu, D. Wang, T. Cui, J. Yin, Y. Wang and J. Zhao, *Anal. Chem.*, 2014, **86**, 11312–11318.
25 H. Peng, M. I. J. Stich, J. Yu, L. Sun, L. H. Fischer and O. S. Wolfbeis, *Adv. Mater.*, 2010, **22**, 716–719.
26 A. M. Badiane, S. Freslon, C. Daiguebonne, Y. Suffren, K. Bernot, G. Calvez, K. Costuas, M. Camara and O. Guillou, *Inorg. Chem.*, 2018, **57**, 3399–3410.
27 J. Bünzli and S. Eliseeva, *Lanthanide Luminescence*, 2011, vol. 7, pp. 1–45.
28 R. E. Whan and G. A. Crosby, *J. Mol. Spectrosc.*, 1962, **8**, 315–327.
29 D. Lu, Z. Hong, J. Xie, X. Kong, L. Long and L. Zheng, *Inorg. Chem.*, 2017, **56**, 12186–12192.
30 S. Uchiyama, A. P. D. Silva and K. Iwai, *J. Chem. Educ.*, 2006, **83**, 720.
31 D. A. Galico and M. Murugesu, *ACS Appl. Mater.*, 2021, **13**, 47052–47060.
32 X. Rao, T. Song, J. Gao, Y. Cui, Y. Yang, C. Wu, B. Chen and G. Qian, *J. Am. Chem. Soc.*, 2013, **135**, 15559–15564.
33 C. D. S. Brites, S. Balabhadra and L. D. Carlos, *Adv. Opt. Mater.*, 2019, **7**, 1801239.